Journal of Solid State Chemistry 182 (2009) 479–483

Contents lists available at ScienceDirect

Journal of Solid State Chemistry

journal homepage: www.elsevier.com/locate/jssc

Structures, phase transitions and microwave dielectric properties of the 6H perovskites $Ba_3BSb_2O_9$, B = Mg, Ca, Sr, Ba

Chris D. Ling [a,b,*], Budwy Rowda [a], Maxim Avdeev [b], Robert Pullar [c]

[a] School of Chemistry, The University of Sydney, Sydney, NSW 2006, Australia
[b] Bragg Institute, ANSTO, PMB 1, Menai, NSW 2234, Australia
[c] Department of Materials, Imperial College London, Exhibition Road, London SW7 2AZ, UK

ARTICLE INFO

Article history:
Received 1 October 2008
Received in revised form
17 November 2008
Accepted 22 November 2008
Available online 3 December 2008

Keywords:
Hexagonal perovskite
Phase diagram
Phase transitions
Dielectric measurements
X-ray diffraction
Neutron diffraction
Thermogravimetric analysis
Differential scanning calorimetry

ABSTRACT

We present a complete temperature-composition phase diagram for $Ba_3BSb_2O_9$, B = Mg, Ca, Sr, Ba, along with their electrical behavior as a function of B. These compounds have long been recognized as 6H-type perovskites, but (with the exception of B = Mg) their exact structures and properties were unknown due to their low symmetries, temperature-dependent phase transitions, and difficulties in synthesizing pure samples. The full range of possible space group symmetries is observed, from ideal hexagonal $P6_3/mmc$ to monoclinic $C2/c$ to triclinic $P\bar{1}$. Direct second-order transitions between these phases are plausible according to group theory, and no evidence was seen for any further intermediate phases. The phase diagram with respect to temperature and the effective ionic radius of B is remarkably symmetrical for B = Mg, Ca, and Sr. For B = Ba, a first-order phase transition to a locally distorted phase allows a metastable hexagonal phase to persist to lower temperatures than expected before decomposing around 600 K. Electrical measurements revealed that dielectric permittivity corrected for porosity does not change significantly as a function of B and is in a good agreement with the values predicted by the Clausius–Mossotti equation.

1. Introduction

Perovskites with large cations such as Ba^{2+} in the 12-fold coordinate A sites have long been of interest for their extreme structural and compositional flexibility. Many of these perovskites adopt the hexagonal 6H structure of which $BaTiO_3$ is the archetype, with BaO_3 layers stacked in an *hcchcc* sequence that results in pairs of face-sharing TiO_6 octahedra alternating with single corner-sharing TiO_6 octahedra.

The present study was prompted by our realization that an entire and fundamental family of these materials—$Ba_3BSb_2O_9$, B = Mg, Ca, Sr, Ba—had been almost completely ignored since being first reported in 1965 [1]. With the exception of the B = Mg case, which adopts the ideal ($P6_3/mmc$) hexagonal $BaTiO_3$ structure [5], none of these materials had ever been purified or had its structure determined. Using variable-temperature synchrotron X-ray powder diffraction (XRD), high-resolution neutron powder diffraction (NPD), and *ab initio* geometry optimization calculations, we recently solved and Rietveld-refined the room temperature structures of $Ba_3MgSb_2O_9$, $Ba_3CaSb_2O_9$ and $Ba_3SrSb_2O_9$ in the successively lower space group symmetries $P6_3/mmc$ (hexagonal), $C2/c$ (monoclinic), and $P\bar{1}$ (triclinic), respectively [2]. These symmetry-lowering distortions appear to be a consequence of internal 'chemical pressure' due to the increasing effective ionic radius (IR) [3] of the alkaline earth cation in the perovskite B-site from Mg^{2+} (IR = 0.72 Å in 6-fold coordination) to Ca^{2+} (IR = 1.00 Å) to Sr^{2+} (IR = 1.18 Å). Increasing the size of B further to Ba^{2+} (IR = 1.35 Å) leads to decomposition at room temperature; however, above T~750 °C $Ba_3BaSb_2O_9$ also adopts an ideal 6H perovskite structure [4] with, to the best of our knowledge, the largest size mismatch ever observed between B-site cations in an ordered hexagonal perovskite (note that Sb^{5+} has IR = 0.60 Å). These structures are shown in Fig. 1, with fundamental crystallographic data summarized in Table 1.

Here, we report the reversal of symmetry-lowering phase transitions on heating, based on variable-temperature XRD and differential scanning calorimetry (DSC), and discuss the kinetics of the transitions. We present our results in a complete phase diagram of $Ba_3BSb_2O_9$ as a function of temperature and IR(B).

In addition to their interesting structural behavior, the antimony based 2:1 perovskites $Ba_3B(Sb_xNb_{1-x})_2O_9$, B = Mg, Zn were recently reported to have attractive microwave dielectric properties [5]. Here, we report the results of dielectric measurements for $Ba_3BSb_2O_9$ with B = Mg, Ca, and Sr.

2. Experimental

Polycrystalline samples of $Ba_3BSb_2O_9$, B = Mg, Ca, Sr, and Ba, were prepared as previously described [2,4,5].

* Corresponding author at: School of Chemistry, The University of Sydney, Sydney, NSW 2006, Australia. Fax: +61 2 9351 3329.
E-mail address: c.ling@chem.usyd.edu.au (C.D. Ling).

0022-4596/$ - see front matter © 2008 Elsevier Inc. All rights reserved.
doi:10.1016/j.jssc.2008.11.026

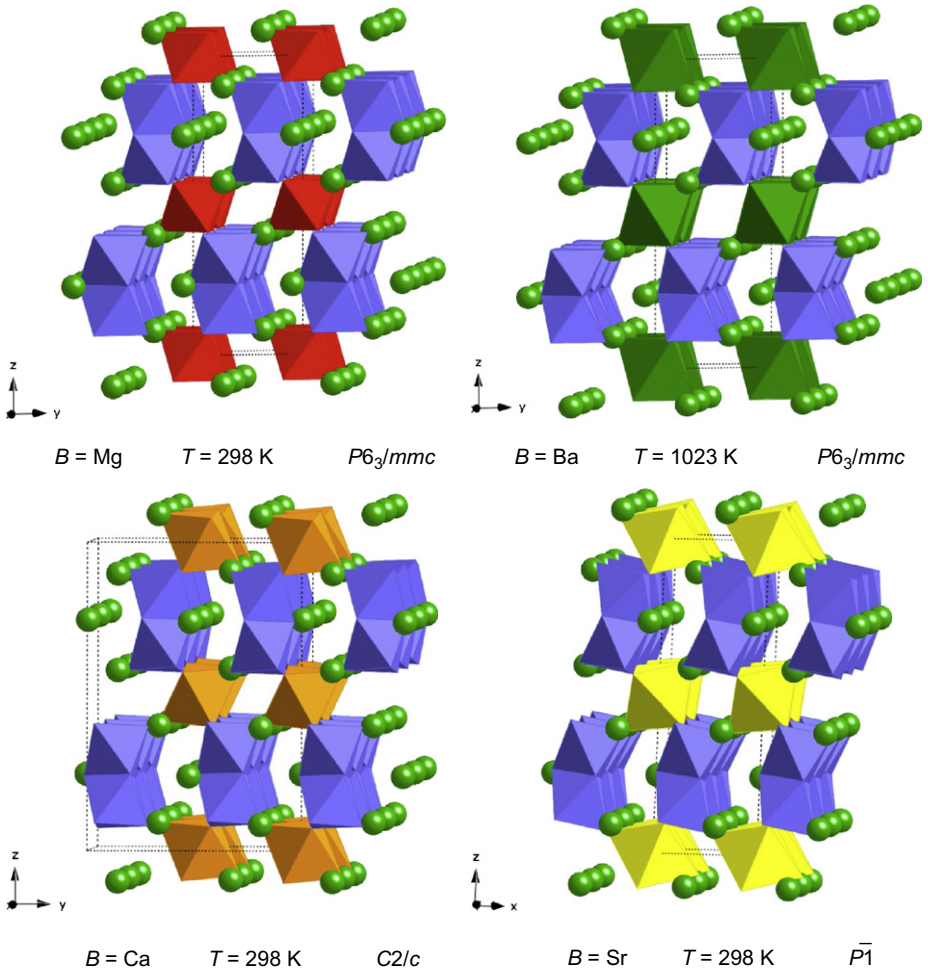

Fig. 1. Structures of $Ba_3BSb_2O_9$, B = Mg, Ca, Sr, and Ba, shown in equivalent projections and on the same scale. Sb_2O_9 face-sharing octahedral dimers are shown as blue polyhedra, and Ba atoms in the perovskite A-sites as green spheres. At T = 298 K, the expansion of the BO_6 octahedra from B = Mg (red) to Ca (orange) to Sr (yellow) cause distortions from hexagonal to monoclinic to triclinic symmetries, respectively. The hexagonal structures of B = Mg at 298 K and B = Ba at 1023 K are also compared (For the interpretation of the references to colour in this figure legend, the reader is reffered to web version of this article).

Table 1
Unit cell and space group data for the room-temperature forms of $Ba_3MgSb_2O_9$, [5] $Ba_3CaSb_2O_9$, [4] and $Ba_3SrSb_2O_9$ [4] and the high-temperature form of $Ba_3BaSb_2O_9$ [2].

Compound	$Ba_3MgSb_2O_9$	$Ba_3CaSb_2O_9$	$Ba_3SrSb_2O_9$	$Ba_3BaSb_2O_9$
Temperature (K)	298	298	298	1023
Space group	$P6_3/mmc$	$C2/c$	$P\bar{1}$	$P6_3/mmc$
Z	2	4	2	2
a (Å)	5.8441 (2)	5.99898 (7)	6.08467 (15)	6.18123 (8)
b (Å)	5.8441	10.37797 (19)	6.08608 (15)	6.18123
c (Å)	14.4089 (6)	14.8658 (3)	15.1934 (3)	15.9900 (3)
α (°)	90	90	89.175 (2)	90
β (°)	90	91.384 (2)	88.485 (2)	90
γ (°)	120	90	119.7431 (11)	120

Variable temperature XRD data were collected on a Panalytical X'Pert Pro powder diffractometer equipped with the Anton-Paar HTK-2000 heating stage (Cu$K\alpha$ radiation). For $Ba_3MgSb_2O_9$, data were collected at room temperature and from 323 to 923 K in 50 K intervals; for $Ba_3CaSb_2O_9$, at room temperature and from 323 to 1473 K in 50 K intervals; for $Ba_3SrSb_2O_9$, at room temperature and from 323 to 1023 K in 50 K intervals; and for $Ba_3BaSb_2O_9$, at room temperature and from 373 to 1273 K in 50 K intervals.

Rietveld-refinements of XRD data were carried out using the GSAS program [6] with the EXPGUI front-end [7]. Scale factors, zero-shifts, background functions (shifted Chebyschev as implemented in GSAS with six terms), peak shape parameters (pseudo-Voigt function "type 4" as implemented in GSAS, refining the Gaussian parameters G_U, G_V and G_W and the Lorentzian parameter L_X) were refined, in addition to unit cell and global isotropic atomic displacement parameters for the structural models used.

DSC data were collected on a Mettler–Toledo DSC823e DSC with a HSS7 sensor.

In order to characterize the dielectric properties of each sample, the quality factor (Q) and relative permittivity (ε_r) were measured at frequencies of ~9 GHz, using its resonant $TE_{01\delta}$ mode. The sample was placed in an oxygen-free high-conductivity copper cavity, supported on a 4 mm high low-loss quartz spacer. The cavity was 30 mm in diameter, with adjustable height. This height was adjusted so that the space above and below the sample was 4 mm, approximately the same as the sample thickness. The diameter of the sample was also approximately $\frac{1}{3}$ of the diameter of the cavity, as recommended by Kajfez and Guillon [8]. The surface resistance of the copper was calculated from the Q value of the TE_{011} resonance of the empty cavity, to allow the results to be corrected for any loss due to the cavity walls. The $TE_{01\delta}$ mode was examined using a Vector Network Analyzer (Hewlett-Packard HP8720D), with a resolution of one Hz. The Q values are corrected

for losses due to the measurement equipment, and so can be assumed to be the Q of the dielectric ceramic. Measurements were made on the as-fired samples, at room temperature. The temperature coefficient of resonant frequency (τ_f) was also obtained, by continuously measuring the variation in resonant frequency (f_r) of the sample between 250 and 300 K, heating and cooling at a rate of 2 K min^{-1}; however, the relatively low density of the pellets used made the results too unreliable to report.

3. Results

Starting from the room-temperature monoclinic $C2/c$ structure of $Ba_3CaSb_2O_9$ [4], we used Rietveld-refinement to determine the monoclinic β angle as a function of temperature from XRD data. Fig. 2 presents the deviation of β from 90° as an order parameter, showing that the phase transition to the ideal hexagonal $P6_3/mmc$ form follows ideal second-order behavior, with a transition temperature of $T = 927 \pm 24$ K.

Variable temperature XRD data for $Ba_3SrSb_2O_9$ revealed two phase transitions on heating, as shown in Fig. 3; from triclinic to monoclinic, and from monoclinic to hexagonal. Rietveld-refinement of a monoclinic $C2/c$ model shows that the monoclinic to hexagonal transition follows ideal second-order behavior, with a transition temperature of $T = 1346 \pm 15$ K (Fig. 1). The triclinic to monoclinic phase transition is indicated by the deviation from linearity of this second order behavior at $T = 409 \pm 12$ K.

Variable temperature XRD data collected on heating a quenched sample of $Ba_3BaSb_2O_9$ (Fig. 4) showed unidentified impurity peaks appearing above T~450 K. The poorly crystalline quenched hexagonal phase was clearly decomposing at this point, demonstrating that it is not the thermodynamic ground state below T~600 K, above which it re-forms. Although the peaks were broad at low temperature, and sharpened on heating, there was no clear peak splitting to indicate symmetry lowering from the ideal high-temperature hexagonal $P6_3/mmc$ form previously refined at 1023 K. However, using Rietveld-refinement to determine the unit cell volume V as a function of temperature, we found a small but clear discontinuity at T~923 K, indicative of a first-order phase transition (Fig. 5). The structural distortions from $P6_3/mmc$ symmetry that must occur in this lower temperature phase could not be reliably determined, with Rietveld-refinement

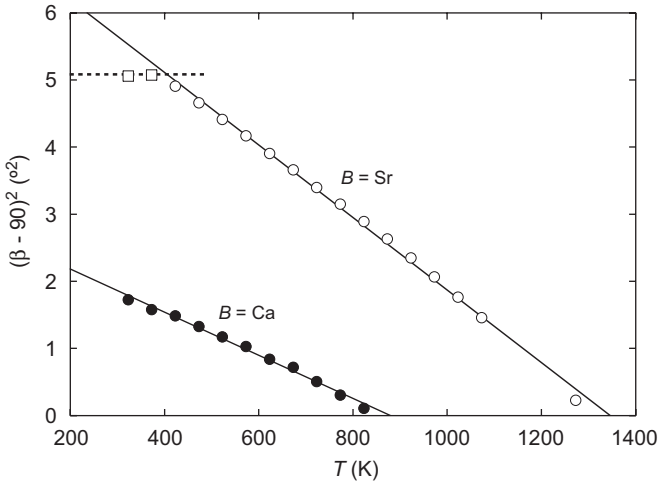

Fig. 2. Variation in the monoclinic β angles (determined by Rietveld refinement of XRD data) for $Ba_3BSb_2O_9$, B = Ca and Sr, as functions of temperature T, used to determine second-order parameters for their phase transitions to hexagonal symmetry ($\beta = 90°$) on heating. Error bars are smaller than symbols. For B = Sr, the transition to triclinic symmetry on cooling is also apparent in the deviation from second-order behavior.

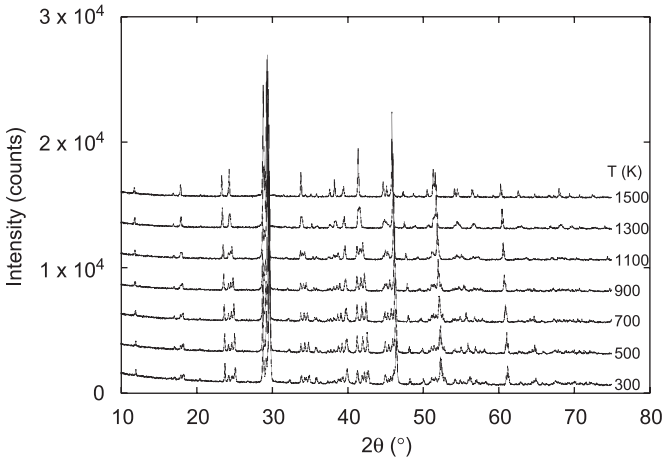

Fig. 3. Selected variable-temperature XRD patterns used to obtain the results shown in Fig. 1 for $Ba_3SrSb_2O_9$. In the 40–44° 2θ range, the monoclinic splitting between 1500 and 1300 K and the triclinic splitting between 500 and 300 K are particularly evident.

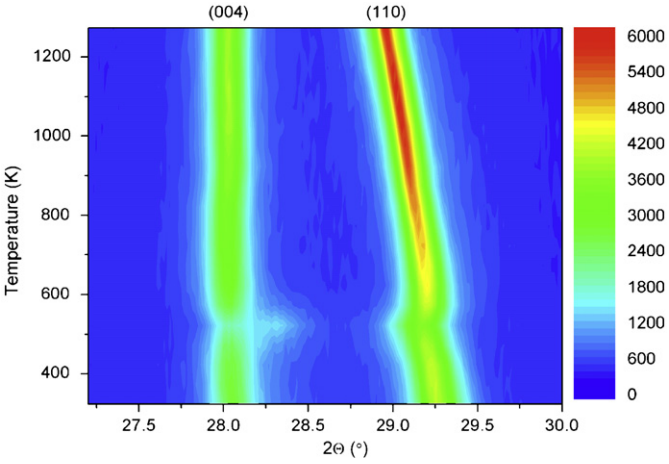

Fig. 4. Contour plot showing the strongest peaks in the XRD data for a quenched sample of $Ba_3BaSb_2O_9$, collected on heating from room temperature. The quenched hexagonal phase decomposes on heating above ~450 K, indicating that it is not thermodynamically stable below ~600 K, above which it reforms.

of the $P6_3/mmc$ model providing an adequate fit to the XRD data. A simultaneous broadening of the diffraction peaks suggests that the distortions are local rather than long-range-ordered.

DSC data collected on heating for $Ba_3BSb_2O_9$, B = Mg, Ca, and Sr, are shown in Fig. 6. Endothermic transitions can be seen in each case. For B = Sr, the observed peak clearly corresponds to the triclinic–monoclinic transition at $T = 409 \pm 12$ K observed in variable temperature XRD data. By analogy, the peak observed for B = Ca at T~240 K can be ascribed to the same transition. For B = Mg, which is still hexagonal at room temperature, the observed peak at T~140 K can be ascribed to the hexagonal–monoclinic transition.

It proved to be difficult to prepare dense ceramics of $Ba_3BSb_2O_9$ for microwave measurements especially in case of B = Ca and Sr. Internal stresses in the material when crossing the $P6_3/mmc$–$C2/c$ phase boundary on cooling caused pellet cracking. Consequently, only the B = Mg compound, which is stable at room temperature in the high symmetry modification, could be sintered at 1473 K, while the B = Ca and Sr compounds were annealed below their first phase transitions above room temperature, i.e., at 773 and 973 K, respectively. The decomposition of the B = Ba compound at

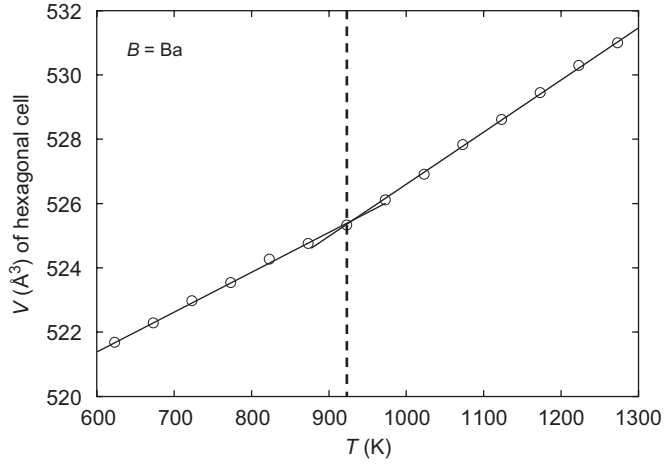

Fig. 5. Unit cell volume V of the ideal hexagonal $P6_3/mmc$ unit cell for $Ba_3BaSb_2O_9$ as a function of temperature T, determined by Rietveld refinement of XRD data. Error bars are smaller than symbols. The first-order transition from an ideal hexagonal to a locally distorted phase on cooling is evidenced by a change in slope at $T \sim 923$ K.

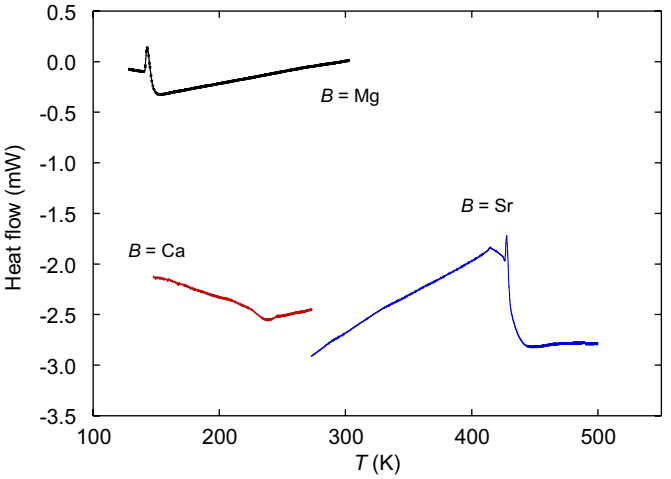

Fig. 6. DSC curves collected on heating for $Ba_3BSb_2O_9$, B = Mg, Ca, and Sr, showing endothermic transitions from monoclinic to hexagonal (B = Mg) and triclinic to monoclinic (B = Ca and Sr).

room temperature meant that quality ceramics could not be prepared and it was not measured. Microwave property measurements for B = Mg, Ca, and Sr were performed on ceramics with relative densities of 75%, 67%, and 72%, respectively. The results are summarized in Table 2. In addition to the experimental values of dielectric permittivity, we also list the values corrected for porosity using Eq. (1) [9] and those predicted by the Clausius–Mossotti equation (Eq. (2)):

$$\varepsilon_{meas} = \varepsilon_{corr}\left(1 - \frac{3P(\varepsilon_{corr}-1)}{2\varepsilon_{corr}+1}\right), \quad (1)$$

$$\varepsilon_{calc} = \frac{3V_m + 8\pi\alpha}{3V_m - 4\pi\alpha}, \quad (2)$$

where ε_{meas} and ε_{corr} are measured and corrected for porosity values of dielectric permittivity, respectively; P is the porosity fraction; V_m is the molar volume (in Å^3); and α is the total polarizability found by applying the additivity rule to the individual ion dielectric polarizabilities tabulated by Shannon [10]. The polarizability for Sb^{5+} is not listed in Ref. [11] and was extrapolated to 2.22 from the values provided for P^{5+} and As^{5+} by

Table 2
Selected physical properties of $Ba_3BSb_2O_9$, B = Mg, Ca, Sr: experimental dielectric permittivity (ε_{meas}), dielectric permittivity corrected for porosity (ε_{corr}), dielectric permittivity calculated with the Clausius–Mossotti equation (ε_{C-M}), and product of the quality factor Q and the resonant frequency f.

B	ε_{meas}	ε_{corr}	ε_{C-M}	f (GHz)	$Q \cdot f$ (GHz)
Mg	9.4	14.2	17.3	8.98	6763
Ca	9.6	17.6	13.9	9.18	3397
Sr	10.6	17.2	12.1	9.05	4676

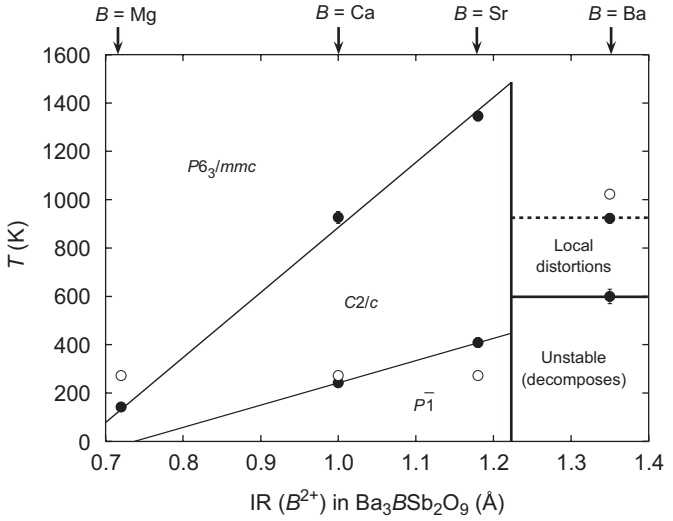

Fig. 7. Thermodynamic phase diagram for $Ba_3BSb_2O_9$, B = Mg, Ca, and Sr, as a function of temperature T and effective ionic radius (IR) of the B^{2+} cation. Open markers represent fully Rietveld-refined structures, and closed markers represent phase transitions determined by variable-temperature XRD ($T > 500$ K) or DSC ($T < 500$ K).

analogy with the polarizabilities of the group 14 elements in the highest oxidation state which demonstrate linear growth in the series $C^{4+} \rightarrow Si^{4+} \rightarrow Sn^{4+}$. The quality factor Q is defined as $Q = 1/\tan\delta$, where δ is dielectric loss.

4. Discussion

The results described above for the 6H perovskites $Ba_3BSb_2O_9$, B = Mg, Ca, Sr, and Ba, can be summarized in a thermodynamic phase diagram as a function of temperature and the effective IR of the B^{2+} cation (Fig. 7). The two parameters have remarkably symmetric effects for B = Mg, Ca, and Sr. In general, $Ba_3BSb_2O_9$ is hexagonal $P6_3/mmc$ at high temperature and small IR(B), and triclinic $P\bar{1}$ at low temperature and large IR(B), passing through an intermediate monoclinic $C2/c$ domain. At constant temperature (298 K), we have shown [4] that the driving force behind the transition from $P6_3/mmc$ to $C2/c$ is the need to alleviate underbonding of Ba^{2+} cations in the perovskite A-site via octahedral rotations, while the transition from $C2/c$ to $P\bar{1}$ is driven by the need to regularize the shape of the Sb_2O_9 face-sharing octahedral dimers. In this study, we have shown that increasing temperature can reverse all these transitions.

A group-theoretical analysis using the program *AMPLIMODES* [11] confirmed the plausibility of the second-order phase transitions observed. from $P6_3/mmc$ to $C2/c$ to $P\bar{1}$. Although two possible intermediate phases exist between $P6_3/mmc$ to $C2/c$ (*Cmcm* and $P\bar{3}1c$), a direct transition is also possible via a Γ^{6+} soft mode. Similarly, the $C2/c$ to $P\bar{1}$ transition can take place either directly or

via an intermediate $P2/c$ phase. No evidence for any of these possible intermediate phases was found in XRD data.

The $B = Ba$ case, with the largest effective ionic radius (IR = 1.35 Å for Ba^{2+} vs. 0.60 Å for Sb^{5+} in 6-fold coordination), shows different phase behavior. The hexagonal $P6_3/mmc$ phase persists to much lower temperatures than expected (albeit with decreasing crystallinity), and the monoclinic $C2/c$ and triclinic $P\bar{1}$ phases are never observed. It appears that these symmetry-lowering modes are insufficient to stabilize the extremely large Ba^{2+} cation in the B site at low temperatures. Below $T\sim923$ K, a subtle but distinct first-order transition takes place to a phase that does not significantly deviate from average $P6_3/mmc$ symmetry. Attempts were made to Rietveld-refine this structure in the possible intermediate space-group symmetries $Cmcm$ and $P\bar{3}1c$, as well as the $P6_3/m$ space group symmetry reported for the 6H perovskites $Ba_3SrNb_2O_9$ and $Ba_3SrTa_2O_9$ [12], but the poor crystallinity of the sample in this temperature range made the results inconclusive while strongly suggesting that the local distortions from $P6_3/mmc$ are not long-range-ordered. Below $T\sim600$ K this locally distorted phase decomposes to a structurally unrelated phase (or phases) too poorly crystalline to identify.

Dielectric permittivity values corrected for sample porosity (Table 2) demonstrate good agreement with those predicted by the Clausius–Mossotti equation and that previously reported for $Ba_3MgSb_2O_9$, 21.5 [5]. The values do not vary significantly from Mg to Sr composition since the higher polarizability of the larger alkaline-earth ion is compensated by the larger molar volume V_m of the material as follows from Eq. (2). The porosity and density variation across the samples are too high to draw reliable conclusion as to whether the B cation type and/or the degree of structural distortion affect the quality factor Q. Low sample density is the most probable reason for the significantly lower value of $Q\cdot f$ found in this study (~6800 GHz, Table 2) compared to that previously measured for $Ba_3MgSb_2O_9$ (~23 000 GHz) [5].

5. Conclusions

The family of 6H perovskites $Ba_3BSb_2O_9$, B = Mg, Ca, Sr, Ba exhibits the full range of possible space group symmetries, from ideal hexagonal $P6_3/mmc$ to monoclinic $C2/c$ to triclinic $P\bar{1}$. Direct second-order transitions between these phases are plausible according to group theory, and no evidence was seen for any further intermediate phases. At constant temperature, the transition from $P6_3/mmc$ to $C2/c$ alleviates underbonding of Ba^{2+} cations in the perovskite A-site via octahedral rotations, while the transition from $C2/c$ to $P\bar{1}$ regularizes the shape of the Sb_2O_9 face-sharing octahedral dimers. At constant chemical pressure (IR(B)), increasing temperature reverses all these transitions. The resulting phase diagram with respect to temperature and IR(B) is remarkably symmetrical for B = Mg, Ca, and Sr. For B = Ba, IR(Ba^{2+}) is too large to be stabilized by the monoclinic or triclinic distortions; instead, a first-order phase transition to a locally distorted phase allows a metastable hexagonal phase to persist to lower temperatures than expected before decomposing around 600 K.

All compositions $Ba_3BSb_2O_9$, B = Mg, Ca, Sr have similar porosity corrected dielectric permittivity ε_{corr} (14.2, 17.6, and 17.1, respectively). The modest $Q\cdot f$ value (~6760, 3400, and 4680 GHz, respectively) is believed to be a result of significant extrinsic losses in low relative density samples.

References

[1] G. Blasse, Journal of Inorganic & Nuclear Chemistry 27 (1965) 993.
[2] B. Rowda, M. Avdeev, P.L. Lee, P.F. Henry, C.D. Ling, Acta Crystallographica Section B—Structural Science 64 (2008) 154.
[3] N.E. Brese, M. O'Keeffe, Acta Crystallographica Section B 47 (1991) 192.
[4] C.D. Ling, M. Avdeev, K. Aivazian, Acta Crystallographica Section B—Structural Science 63 (2007) 584.
[5] M.W. Lufaso, E. Hopkins, S.M. Bell, A. Llobet, Chemistry of Materials 17 (2005) 4250.
[6] A.C. Larson, R.B. Von Dreele, Los Alamos National Laboratory Report LAUR 86-748, 1994.
[7] B.H. Toby, Journal of Applied Crystallography 34 (2001) 210.
[8] D. Kajfez, P. Guillon, Dielectric Resonators, Noble Publishing Corporation, Georgia, USA, 1998, p. 327.
[9] S.J. Penn, N.M. Alford, A. Templeton, X.R. Wang, M.S. Xu, M. Reece, K. Schrapel, Journal of the American Ceramic Society 80 (1997) 1885.
[10] R.D. Shannon, Journal of Applied Physics 73 (1993) 348.
[11] M.I. Aroyo, J.M. Perez-Mato, C. Capillas, E. Kroumova, S. Ivantchev, G. Madariaga, A. Kirov, H. Wondratschek, Zeitschrift Fur Kristallographie 221 (2006) 15.
[12] H.W. Zandbergen, D.J.W. Ijdo, Acta Crystallographica Section C—Crystal Structure Communications 39 (1983) 829.